THE ASTROPHYSICAL JOURNAL, 307:431–440, 1986 August 15

THEORETICAL MODELS FOR H II REGIONS. II. THE EXTRAGALACTIC H II REGION ABUNDANCE SEQUENCE

M. A. DOPITA AND I. N. EVANS
Mount Stromlo and Siding Spring Observatories, The Australian National University
Received 1985 October 7; accepted 1986 February 5

ABSTRACT

With the aid of the extensive, homogeneous grid of theoretical photoionization models described in the first paper of this series, we have generated a multiline fit to the observed emission-line spectral sequence of extragalactic H II regions. It is possible to produce an excellent fit between the (rather narrow) emission-line ratio sequences that are observed and the theoretical sequences, provided that the average ionization parameter is strongly coupled with metallicity, and provided that nitrogen is a product of secondary nucleosynthesis.

Using this theoretical sequence of H II region models, we have recalibrated the semiempirical abundance diagnostic ratios used by Alloin *et al.* (1979), Pagel *et al.* (1979), and McCall, Rybski, and Shields (1985) and have generated new abundance diagnostic ratios. We find that the correlation between ionization parameter and abundance has the effect of changing the previous abundance calibration toward lower abundances, particularly for the most metal-rich H II regions. Finally, we give a new technique to derive abundances from H II region spectra.

Subject headings: galaxies: evolution — nebulae: abundances — nebulae: H II regions

I. INTRODUCTION

The spectrophotometry of giant H II regions in external galaxies has been the principal datum used to derive the abundances and abundance gradients of elements lighter than calcium. Since these elements, in particular oxygen and neon, are produced in the massive Population I stars, the interpretation of the observational material is of fundamental importance to our understanding of the evolution of galaxies.

In the past, much effort has been devoted to attempts to derive explicit elemental abundances from very high signal-to-noise spectra of individual H II regions. Formerly, the semiempirical ionization correction factor technique pioneered by Peimbert and Costero (1969) has been employed with considerable success to derive abundances in many galaxies (e.g., Peimbert and Torres-Peimbert 1974, 1976; Dufour 1975, 1977; Smith 1975; Pagel *et al.* 1978; Lequeux *et al.* 1979). More recently, as theoretical photoionization models have improved, these have been applied toward direct derivation of the abundances of individual H II regions (e.g., Shields and Searle 1978; Dufour *et al.* 1980; Dufour, Shields, and Talbot 1982). However, both of these methods depend critically on the detection of the temperature-sensitive line [O III] λ4363, which is very weak in, or entirely absent from, the spectra of metal-rich H II regions.

An alternative avenue of approach to the abundance problem is suggested by the fact that the spectra of extragalactic H II regions appear to represent a one-parameter sequence. This was first suggested by Searle (1971) who felt that the excitation, being probably controlled by the oxygen abundance, would represent an appropriate classification index. Sarazin (1976) developed this idea and attempted to fit the whole sequence with theoretical models. He concluded that, in addition to the abundance variation, there must also be an excitation variation or a softening of the radiation field at higher metallicity. As more data have been accumulated, this sequence of H II region spectra has looked better (see, for example, the compilation by Baldwin, Phillips, and Terlevich 1981, or the very large sample of McCall, Rybski, and Shields 1985). The major question therefore revolves around what is the most appropriate emission-line ratio to use for abundance sequencing. Pagel *et al.* (1979) have suggested that the ratio ([O II] λ3727 + [O III] $\lambda\lambda$4959, 5007)/Hβ is better than [O III] $\lambda\lambda$4959, 5007/Hβ because it is less sensitive to the geometry of the gas distribution with respect to the ionizing radiation. This appears to be amply borne out by further observation (Pagel, Edmunds, and Smith 1980; Edmunds and Pagel 1984; McCall, Rybski, and Shields 1985).

To derive an absolute abundance from such a sequence is more difficult. Pagel and his co-workers rely heavily on model fits to a metal-rich H II region in M101, S5, to fix the abundance scale at the upper end. In the third paper in this series (Evans 1986; hereafter Paper III) we will show that this "fiducial" point may be seriously misplaced. Alloin *et al.* (1979) argue that a safer approach may be to determine the electron temperature in the O^{++} zone via a semiempirical route involving the [O III] $\lambda\lambda$4959, 5007/[N II] $\lambda\lambda$6548, 6584 ratio and then to derive the oxygen abundance from the abundance–electron temperature correlation. However, the success of this method depends critically on the assumed nucleosynthetic origin of nitrogen, which has been variously argued to be either a primary or secondary element (see § IV below).

In the first paper of this series (Evans and Dopita 1985; hereafter Paper I), we described computation of an extensive grid of models directed toward the production of a set of diagnostic diagrams which would enable the ionization parameter of H II regions and the ionization temperature of their exciting stars to be estimated in a manner that is largely independent of nebular and stellar chemical abundances. This is an essential first step toward the correct theoretical calibration of the abundance scale of extragalactic H II regions. In Paper I we discovered that the ionization temperature of the stars showed remarkably little variation with abundance, within the limitations of the available data, but that the ionization parameter

shows a strong inverse correlation with metallicity. In this paper we will use this result as the starting point of an attempt to fit simultaneously all the important line ratios observed in extragalactic H II regions. As a result, we are able to both calibrate the abundance sequence in an absolute manner and to suggest new abundance sequencing ratios which may be useful from an observational view point.

II. THE OBSERVATIONAL DATA BASE

In this paper we follow Paper I in selecting for the data base the compilation of Baldwin, Phillips, and Terlevich (1981; hereafter BPT) and the very extensive homogeneous data set of McCall (1982) which is substantially that published by McCall, Rybski, and Shields (1985). The BPT set is composed of most of the published high-quality data available to them. This sample has severe selection effects. For example, it is strongly biased toward the highest surface brightness H II regions in the Magellanic Clouds, blue compact galaxies, and giant H II regions (such as NGC 604 in M33) which tend to occur in the outer parts of their parent galaxies. This in turn means that the sample is strongly biased toward lower abundance objects. The McCall (1982) sample is much more representative of the H II region population. Galaxies were selected on the basis of high equivalent width of Hα and at various radial positions within the galaxies. However, the galaxies chosen tend to be of high absolute magnitude, and this fact, together with the fact that the sample is rich in H II regions in the inner parts of galaxies, means that many more high-abundance objects were observed. Thus the two samples are somewhat complementary for the purpose of ensuring a good coverage over a wide range of abundances.

III. THE THEORETICAL MODELS

A full description of the theoretical photoionization models used here is given in Paper I. Suffice it to say here that the basic grid of models consists of steady state spherically symmetric dust-free nebulae of uniform density of hydrogen atoms plus ions (10 cm^{-3}) and constant helium abundance. The density is chosen to be sufficiently low as to preclude the possibility of collisional de-excitation of optical forbidden lines. The central ionizing OB association was approximated by a stellar atmosphere photon source with a single ionization temperature and the metallicity of the stellar atmosphere was kept the same as the surrounding nebula. The log $g = 4.0$ models of Hummer and Mihalas (1970) were used with the interpolation scheme developed by Shields and Searle (1978).

With these assumptions, the three parameters that have a major effect on the emission-line spectrum are chemical abundance, ionization parameter, and ionization temperature of the exciting stars. Our basic net of models, described in Paper I, was cast wide enough to encompass all the likely values of these parameters and all the variety of the observed spectra.

Three subsidiary grids were also developed to gain an understanding of the effects of changing element abundance ratios on the emission-line spectrum. Specifically, these were (i) a grid allowing changes in the (C + Mg + Si)/O ratio to investigate the effects of depletion onto refractory grains, (ii) a grid allowing changes in the N/O ratio to investigate the nucleogenic status of nitrogen, and (iii) a grid allowing changes in the S/O ratio, which may reflect the initial mass function (IMF) for the more massive stars. Together, these grids offer an excellent insight into the spectral characteristics of H II regions and render it feasible to attempt a multiparameter fit to the observed spectral sequence in external galaxies.

IV. FITTING PROCEDURE

a) *Initial Assumptions*

In Paper I, we developed a set of diagnostic diagrams to enable the ionization parameter of the H II region and the ionization temperature of the central star to be determined largely independently of the chemical abundance in the nebula. These diagrams involved line ratios formed principally from the [O I], [O II], [O III], [S II], and [S III] lines, as well as the Balmer lines of hydrogen. Unfortunately, the data base is very sparse in measurements of the [O I] λ6300 line and the [S III] λ9069 line, and so a satisfactory diagnosis is possible over relatively few H II regions. However, this was sufficient to show that the ionization parameter varies over a very wide range of nearly two orders of magnitude. However, the ionization temperature does not show great variability, the data points clustering about $T_{ion} = 41{,}500$ K with a total scatter of order 3000 K. There is no evidence to support the idea that the ionization temperature and the ionization parameter are coupled in the H II regions for which a complete analysis was possible.

Using the first excitation diagram of BPT, in which the [O II]/[O III] forbidden line ratio, log (3727/5007), is plotted against log (5007/4861), the distribution of the observational points can be reconciled with the theoretical curves only if the ionization parameter is itself correlated with metallicity. The sense of this is that high chemical abundance is correlated with low ionization parameter.

On the basis of Paper I, we take as the point of departure for the fitting process a fixed ionization temperature of 41,500 K, and an assumed correlation between ionization parameter, $\bar{Q}$(H) (defined in Paper I), and chemical abundance, 12 + log (O/H). The next problem is to discover the form of this correlation.

b) *The $\bar{Q}$(H) − Z Correlation*

In Paper I, we found that by far the best $\bar{Q}$(H) indicator is the composite line ratio involving the forbidden lines of sulfur, (6731 · 6731/6563 · 9069). This ratio changes by 1.5 magnitudes for every magnitude change in $\bar{Q}$(H) and is substantially independent of ionization temperature or Z. Unfortunately, the data base on the [S III] λ9069 line is essentially nonexistent. Fortunately, it is the [S II] λ6731 line that is the most sensitive to $\bar{Q}$(H), so that the simple ratio (6731/6563) is still adequate as a $\bar{Q}$(H) discriminant, provided that $\bar{Q}$(H) is not too low or that the abundance of sulfur relative to oxygen is not greatly variable.

In Figure 1, we plot the [S II] λ6731/Hα ratio against the Pagel *et al.* (1979) abundance discriminant ([O II] λ3727 + [O III] λλ4959, 5007)/Hβ. The theoretical grid is for an ionization temperature of 41,500 K and varying $\bar{Q}$(H) and Z. The $\bar{Q}$(H)–Z correlation is evident in this diagram. However, at the relatively low values of $\bar{Q}$(H) which characterize the bulk of H II regions, the Pagel *et al.* (1979) abundance discriminant begins to compact and become ambiguous. We therefore require to find an abundance indicator that does not suffer from this problem.

We find that the Alloin *et al.* (1979) discriminant ratio [O III] λλ4959, 5007/[N II] λλ6548, 6584 is not very helpful, at least at this stage, because it is very dependent on the assumed

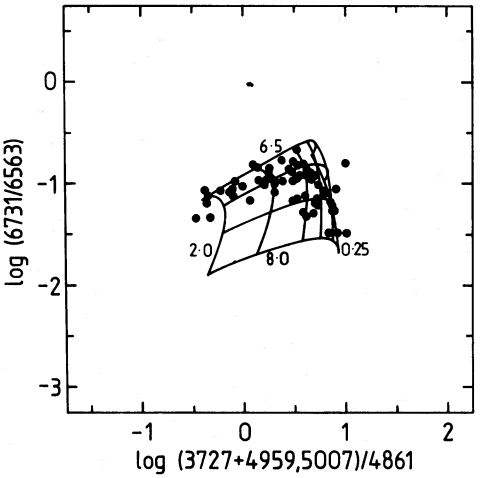

FIG. 1.—The simple $\bar{Q}$(H) discriminant, (6731/6563) plotted against the Pagel *et al.* (1979) abundance sensitive ratio ([O II] λ3727 + [O III] $\lambda\lambda$4959, 5007)/Hβ. The theoretical grid of models is for an ionization temperature of 41,500 K, and elemental abundances as defined in Table 1. Lines of constant mean ionization parameter log $\bar{Q}$(H) = 6.5 cm s^{-1} and log $\bar{Q}$(H) = 8.0 cm s^{-1} are labeled with 6.5 and 8.0, respectively, with intermediate values log $\bar{Q}$(H) = 7.0 and 7.5 cm s^{-1} also shown. Lines of constant metallicity Z = 1/4, 1/2, 3/4, 3/2, and 2 $Z_\odot$ are illustrated. The positions of H II regions in our observational data base are indicated by filled circles.

nucleogenic status of nitrogen, and furthermore the [O III] line strength is dependent on $\bar{Q}$(H).

The conditions required to obtain a useful abundance indicator are that it must involve only the bright optical lines between 3727 Å and 6731 Å, it should retain sensitivity at high abundance where the [O III] lines become weak or absent, and it should not use the [N II] lines. Thus, the only possible lines that can be used are the [O II], [S II], and Balmer lines. By trial and error we discovered that the composite ratio (3727 · 3727/4861 · 6731) is very suitable, since it shows good Z sensitivity throughout the range encompassed by the observed H II regions, shows very little sensitivity to $\bar{Q}$(H), and is only slightly more sensitive to variations in the ionization temperature than the Pagel *et al.* (1979) abundance indicator. In Figure 2, we plot the [S II] λ6731/Hα ratio against this abundance discriminant. The $\bar{Q}$(H)–Z correlation is now clear and unambiguous.

It might be argued that sulfur abundance variations could produce the correlation of Figure 2. However, if this were so, we would require a massive variation on the S/O ratio; sulfur would have to be at least a secondary nucleosynthetic element. Such a conclusion would be completely at variance with what we know about the nucleogenic origin of sulfur (Weaver, Zimmerman, and Woosley 1978; Clegg, Lambert, and Tomkin 1981; Nomoto, Thielemann, and Yokoi 1984) and with a detailed analysis of observational results on supernova remnants (Dopita *et al.* 1984), of H II regions (Dennefeld and Stasińska 1983), and planetary nebulae in our own Galaxy (Kaler 1981). These studies show no detectable variations in S/O abundance ratios. If we assume that the S/O abundance ratio is fixed, then Figure 2 can be used to derive the $\bar{Q}$(H)–Z relationship. However, we need the absolute value of the S/O abundance ratio to be able to do this, since the $\bar{Q}$(H) value derived in Figure 2 is very sensitive to the assumed S/O abundance ratio. Fortunately, the first of the BPT diagrams, which depends only on line ratios of oxygen ions, is also useful as a $\bar{Q}$(H)–Z discriminant, provided that the assumption of constant ionization temperature is valid. We plot this in Figure 3. The separation is not as good as in Figure 2, but the trend and mean value can be derived. The discrepancy between the loci of the observational points in Figures 2 and 3 is largely due to the fact that the data sample in Figure 2 is incomplete at high values of $\bar{Q}$(H) (low Z) because the [S II] λ6731 line is either too weak to be measured or has very large errors for the low abundance objects in the BPT data base. Nevertheless, there is some degree of inconsistency between the figures. A possible cause for this may be due to uncertainty in the rate of the $H^0 + O^{++} \rightleftharpoons H^+ + O^+$ charge exchange reaction, which will weaken I([O III] λ5007) at lower values of $\bar{Q}$(H) because of the presence of partially ionized gas. The inconsistencies between the figures cannot be significant, however, since the abundance sequence derived below accurately tracks the locus of observed H II regions, and the chemical abundances derived from independent diagnostic line ratios are internally consistent to within the errors.

We have used Figure 2 to extract the form of the $\bar{Q}$(H)–Z relation, and Figure 3 to extract the S/O abundance ratio

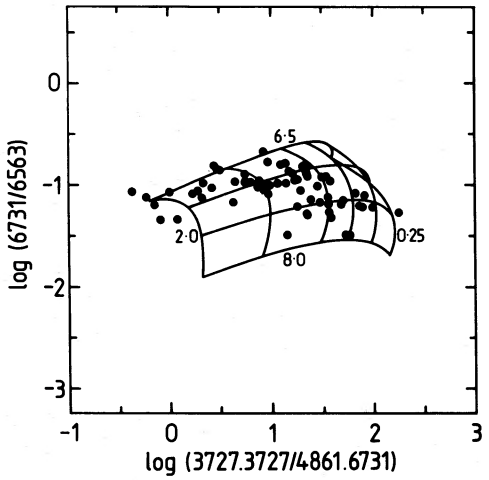

FIG. 2.—As Fig. 1, but employing the abundance discriminant suggested in the text, (3727 · 3727/4861 · 6731).

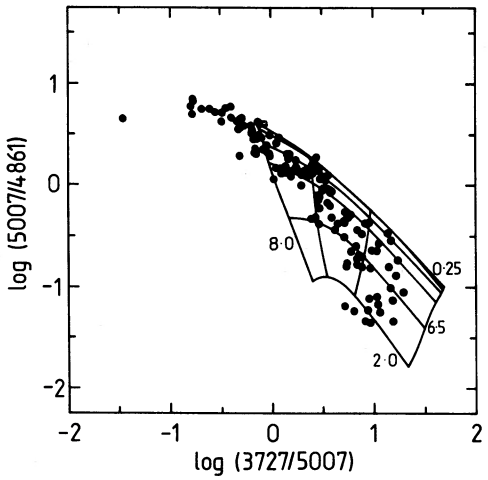

FIG. 3.—As Fig. 1, but for the first of the BPT diagrams, (5007/4861) vs. (3727/5007).

which renders Figures 2 and 3 most nearly self-consistent. We have fitted the data to the simple functional form

$$12 + \log (\mathrm{O/H}) = A - B \times \log \bar{Q}(\mathrm{H}),$$

$$\bar{Q}(\mathrm{H})_{\min} < \bar{Q}(\mathrm{H}) < \bar{Q}(\mathrm{H})_{\max} ,$$

where $A = 13.15$, $B = 0.5903$, $\log \bar{Q}(\mathrm{H})_{\min} = 6.7$, and $\log \bar{Q}(\mathrm{H})_{\max} = 8.4$, respectively. Within the substantial scatter at a given Z, this represents a very good fit to the observations. The accuracy with which the oxygen abundance can be derived from the abundance sequence, together with an example of its application to H II regions in the spiral galaxy M101, is discussed in Paper III.

The question of why there should be a $\bar{Q}(\mathrm{H})$–Z correlation is important enough to warrant a digression at this point. The possible explanations are (i) there is a correlation between the IMF and Z, (ii) the correlation is the result of dust absorption, and (iii) there are environmental effects which change the "geometry" at high Z.

In Paper I we have already discussed the first of these alternatives, and will not develop it further here.

The second alternative is related to a suggestion by Sarazin (1976) that the excitation gradients seen in H II regions are the result of nongray dust absorption. Certainly, if the dust has an absorption curve that is an increasing function of frequency, this will very effectively "soften" the radiation field and give rise to low-excitation H II regions in dusty environments. The dusty models of Sarazin (1976, 1977), Dufour *et al.* (1980), and Stasińska (1980) have many characteristics of dust-free models with a lower ionization temperature, but this is because of the unrealistic assumption that the dust absorption cross section varies as ν or ν^2. It seems most likely that actual dust has an absorption peaked at $\sim$16–17 eV, falling off at higher frequencies (Martin and Ferland 1980). This behavior makes the net stellar radiation which is absorbed by the gas appear to be harder than that emitted by the star; that is, it makes the star look hotter than it really is. Increasing the amount of "real" dust (based on current predictions of its UV cross sections) makes $\bar{Q}(\mathrm{H})$ apparently *increase* by making the star appear to be hotter, which is the opposite of the observed $\bar{Q}(\mathrm{H})$–Z correlation. We emphasize again that we found no strong evidence to support the idea of a varying ionization temperature. Thus if dust absorption is important in driving a $\bar{Q}(\mathrm{H})$–Z correlation, it must be through it possessing a gray rather than frequency-dependent opacity. Petrosian, Silk, and Field (1972) have developed analytic approximations to the ionization balance of dusty Strömgren spheres. If, within an H II region, a fraction f of the stellar ionizing photons is absorbed by the gas, then the mean ionization parameter is approximately given by

$$\bar{Q}(\mathrm{H}) = fL_C/4\pi(y_0 R/2)^2 N , \quad (1)$$

where L_C is the luminosity of the star in ionizing photons per second, R is the dust-free Strömgren radius, and y_0 is the fractional radius of the ionized zone, compared with the Strömgren radius, in the presence of dust. Equation (8) of Petrosian, Silk, and Field (1972) gives an expression for f and y_0. Although $\bar{Q}(\mathrm{H})$ does indeed decrease with increasing dust content, the rate of variation is slow, and unreasonably large values of dust absorption would be required to produce the observed correlation of $\bar{Q}(\mathrm{H})$ and Z. We therefore conclude that dust absorption effects are not primarily responsible.

The third possibility, that environmental effects cause a changing $\bar{Q}(\mathrm{H})$, is probably the most likely explanation. In general, H II regions are selected for observation because they have a high surface brightness. The surface brightness and the $\bar{Q}(\mathrm{H})$ values are correlated. The Strömgren condition is

$$L_C = (4\pi/3)R^3 N^2 \epsilon \alpha_B , \quad (2)$$

where ϵ is the volume filling factor and α_B is the effective recombination coefficient for hydrogen. The mean surface flux at Hβ is given by

$$S_{\mathrm{H}\beta} = (4/3)RN_{\mathrm{H}}^2 \epsilon \alpha_{\mathrm{eff}} h\nu_{\mathrm{H}\beta} , \quad (3)$$

where α_{eff} is the effective recombination coefficient for Hβ. Combining equations (1)–(3) we have, for a dust-free H II region,

$$S_{\mathrm{H}\beta} = \bar{Q}(\mathrm{H})(N_{\mathrm{H}}^2/N)(\alpha_{\mathrm{eff}}/\alpha_B)h\nu_{\mathrm{H}\beta} \quad (4)$$

$$\approx \bar{Q}(\mathrm{H})\{N/[1 + Z(\mathrm{He})]^2\}(\alpha_{\mathrm{eff}}/\alpha_B)h\nu_{\mathrm{H}\beta} , \quad (5)$$

since $N \approx N_{\mathrm{H}}[1 + Z(\mathrm{He})]$, where $Z(\mathrm{He})$ is the relative abundance of helium by number with respect to hydrogen, and we have assumed helium to be singly ionized. Equations (4) and (5) show that high-density, high-$\bar{Q}(\mathrm{H})$ H II regions will be preferentially observed. Since such H II regions are not observed in the high-Z regime, we must conclude that there is a real absence of high-$\bar{Q}(\mathrm{H})$, high-Z objects in galaxies. The most obvious physical reason for this might be that the mean density of H II regions increases in the inner regions of galaxies where high values of Z are located. This is not unreasonable, since the surface density of gas tends to increase in these regions (Paper III). An alternative explanation might be that the specific rate of star formation of massive stars is lower in high-Z regions, and thus the mean value of L_* is lower. These two alternatives could be discriminated between by a program of absolute photometry in the Balmer lines. The referee suggested an alternative explanation, namely, that ϵ decreases with Z. Presumably, ϵ is not unity because most of the volume of the H II region is occupied by shocked stellar wind, which is in turn accelerated by radiation pressure on heavy element ions in the stellar atmosphere, yielding a correlation between volume filling factor and metallicity.

c) *Nucleogenic Status of Nitrogen*

A question that has been discussed for many years is whether nitrogen is enriched as a primary element (in which case N/O is constant) or whether it is a secondary element (which implies N/O varying as O/H; Talbot and Arnett 1974). The evidence from supernova remnants implies a secondary origin (Dopita *et al.* 1984), and the secondary nature of nitrogen has already been suggested for H II regions (Dufour, Shields, and Talbot 1982; Mathis, Chu, and Peterson 1985). On the other hand, H II region data have suggested that a primary enrichment component is present, but that this varies in its importance from galaxy to galaxy (Smith 1975; Edmunds and Pagel 1978; Pagel *et al.* 1978; Alloin *et al.* 1979; Pagel and Edmunds 1981).

Since we have now established a statistical relationship between T_{ion}, $\bar{Q}(\mathrm{H})$, and Z, we are now in a position to examine this question. The diagnostic diagrams of BPT which involve [N II] ratios are not particulary useful in this regard, since a clean separation of the various parameters is not possible. However, the ratio [O II] λ3727/[N II] λ6584 is much more useful, since this is sensitive to the N/O ratio, but depends less on the other parameters. In Figure 4, we plot this ratio against our abundance discriminant (3727 · 3727/4861 · 6731). The

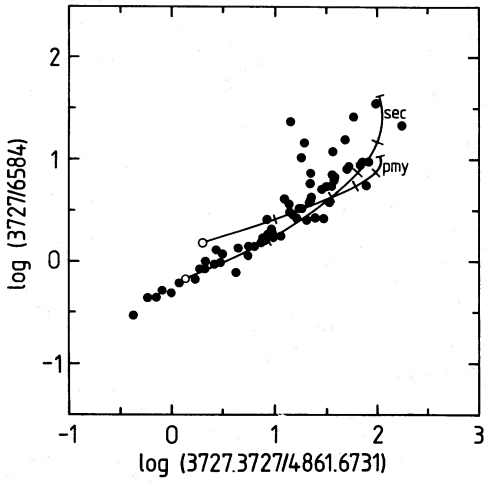

FIG. 4.—Theoretical sequences employing the $\bar{Q}$(H)–Z relationship derived in the text and "solar" abundance ratios given in Table 1, showing the difference between primary and secondary nitrogen enrichment for the line ratio (3727/6584) vs. (3727 · 3727/4861 · 6731). Both sequences are normalized to the same N/O ratio at solar oxygen abundance. Tick marks indicate metallicities of Z = 1/4, 1/2, 3/4, and 3/2 $Z_\odot$, while open circles indicate a metallicity of 2 $Z_\odot$. Positions of H II regions in our observational data base are indicated by filled circles.

observed points show very little scatter in the high abundance limit, which suggests that at this limit, at least, the various galaxies share a common mode of nitrogen enrichment. The two theoretical sequences shown are for nitrogen assumed primary, with a solar N/O ratio at solar abundance, and for nitrogen assumed secondary, likewise with a solar N/O ratio at solar abundance. Clearly, the latter curve is a much better fit to the observed points, which strongly argues for nitrogen as a secondary element, at least at high Z. The large amount of scatter at the low-Z end is real and indicates that there is a different source of nitrogen enrichment in this abundance regime.

The ratio [O III] $\lambda\lambda$4959, 5007/[N II] $\lambda\lambda$6548, 6584, which was used by Alloin *et al.* (1979) as a nebular temperature indicator, and therefore indirectly as an abundance indicator, shows considerable scatter when plotted against our abundance indicator (Fig. 5, in which the two theoretical curves are

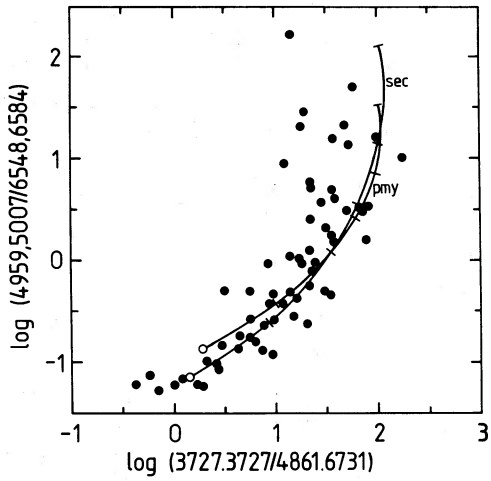

FIG. 5.—As Fig. 4, but for the Alloin *et al.* (1979) abundance sensitive line ratio [O III] $\lambda\lambda$4959, 5007/[N II] $\lambda\lambda$6548, 6584 vs. (3727 · 3727/4861 · 6731).

similar to those of Fig. 4). Also, note that the total range covered by the observed H II regions in the Alloin *et al.* (1979) ratio is much greater than in the [O II] λ3727/[N II] λ6584 ratio, but that the differences between the theoretical sequences for primary and secondary nitrogen enrichment are considerably smaller in Figure 5 than in Figure 4. The physical reason for both the scatter of the points and this range is that the Alloin *et al.* (1979) ratio is very sensitive to the value of $\bar{Q}$(H). The range therefore reflects the $\bar{Q}$(H)–Z correlation and the scatter the intrinsic scatter in the value of $\bar{Q}$(H) at any given abundance. Without a proper relationship between $\bar{Q}$(H) and Z, the nucleogenic status of nitrogen becomes uncertain.

The measurement of the nitrogen yield relative to the oxygen yield in individual galaxies can be used as a method of investigating the stellar initial mass function. According to the theory of Renzini and Voli (1981), nitrogen is synthesized in stars of 4–8 solar masses during various dredge-up phases. On the other hand, the oxygen yield is controlled by the rate of production of massive stars, so that, given an adequate theoretical basis, a secondary nitrogen yield can be used to put an observational constraint on the relative time-integrated star formation rates of intermediate mass stars and stars in the 15–50 solar mass range. However, only the first and second dredge-up phases produce secondary nitrogen. Renzini and Voli (1981) point out that when the third dredge-up phase occurs in conjunction with hot-bottom burning, primary nitrogen can be produced. This will occur for stars with a mass greater than some critical value, $\sim$6.8 solar masses. Thus, scatter in the N/O–O relation can be caused by a variation in this primary yield and will be a measure of the relative enrichment resulting from the more massive and less massive intermediate mass stars. An alternative source of primary nitrogen is by direct production in supermassive stars (Woosley and Weaver 1982).

The scatter at the low-abundance end of Figure 4 is similar to, although less extreme than, that found by Pagel and Edmunds (1981). It appears that the more massive disk galaxies conform to a purely secondary slope down to low abundance, but that low-mass irregulars and blue compact galaxies have N/O ratios which tend to be systematically lower at a given O abundance. From the above discussion, this could be either the result of a shallower IMF in the latter group, or a result of a variable efficiency of dredge-up in the hot-bottom burning phase, or a result of a past burst of supermassive star formation in the more massive galaxies.

V. COMPARISON WITH OBSERVATIONS

Following the procedure outlined in the previous section we have generated a theoretical sequence of H II regions that should reproduce the observed relative intensities of the [O II], [O III], [S II], [N II], and Balmer lines. This sequence is characterized by a constant ionization temperature, $T_{\rm ion}$ = 41,500 K, and the adopted set of elemental abundances given in Table 1 for "solar" composition. All abundance ratios are kept in their solar ratios at other metallicities, except for nitrogen which is treated as a secondary element with respect to oxygen. The adopted $\bar{Q}$(H) versus oxygen abundance is

$$\log \bar{Q}(\mathrm{H}) = 22.28 - 1.694 \times [12 + \log (\mathrm{O/H})] ,$$

$$8.20 \lesssim 12 + \log (\mathrm{O/H}) \lesssim 9.20 .$$

We will now show that this sequence does in fact reproduce the observations in the diagnostic plots that are commonly used for excitation and abundance diagnostics.

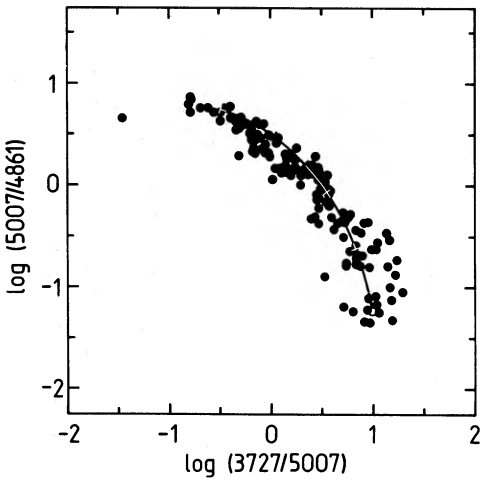

FIG. 6.—The final theoretical sequence plotted on the first BPT figure, (5007/4861) vs. (3727/5007).

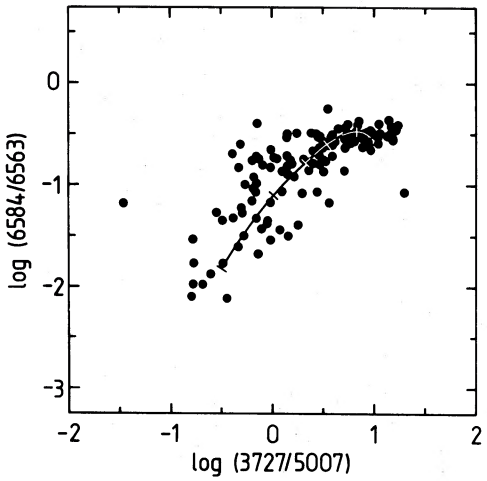

FIG. 7.—As Fig. 6, but for the second BPT figure, (6584/6563) vs. (3727/5007).

a) Excitation Diagrams of Baldwin, Phillips, and Terlevich

The first of these, the plot of (5007/4861) versus (3727/5007), was used to derive the S/O abundance ratio (Fig. 3, above) and therefore should *a priori* yield a good fit to the observational data. To confirm this, we compare the final sequence of models to the observations in Figure 6. The excitation diagrams which use the [N II] lines are useful as a check that we have correctly solved the nitrogen abundance problem. The sequence of models is compared with the observations on the (6584/6563) versus (3727/5007) and the (5007/4861) versus (6584/6563) line ratio diagrams in Figures 7 and 8.

b) Pagel et al. and Alloin et al. Abundance Indicators

We have already pointed out that the Pagel *et al.* (1979) abundance indicator is also sensitive to $\bar{Q}$(H). However, the effect of the $\bar{Q}$(H)–Z correlation we have derived is to enhance the utility of the ([O II] λ3727 + [O III] $\lambda\lambda$4959, 5007)/Hβ ratio as an abundance indicator. The physical reason for this is because, at constant $\bar{Q}$(H), the electron temperature of the nebula increases as the oxygen abundance decreases. Since the flux in the forbidden lines increases rapidly with electron temperature and the effective recombination rate for hydrogen decreases with electron temperature, the Pagel *et al.* (1979) ratio increases with decreasing abundance. However, this trend cannot continue indefinitely, and the ratio maximizes at some particular metal abundance. The forbidden line emission maximizes when the collisional excitation rate peaks and decreases at lower abundances (higher T_e) where free-free and H, He recombination cooling dominate the forbidden lines. The effect of superposing a $\bar{Q}$(H)–Z correlation is to push this maximum toward lower metallicity, so increasing the abundance range over which the Pagel *et al.* (1979) ratio is monotonic in its behavior. In Figure 9, we plot the Pagel *et al.* (1979) ratio against our own abundance sensitive ratio, (3727 · 3727/4861 · 6731). Clearly, the theoretical sequence is an excellent fit to the observed sequence.

A consequence of the $\bar{Q}$(H)–Z correlation is to change the absolute calibration of the abundance scale of H II regions, particularly at high Z. This occurs because the lower $\bar{Q}$(H) at the high metallicity extreme allows the electron temperature to fall, and so quench the optical forbidden lines. For an oxygen abundance 12 + log (O/H) much greater than 9.2, the H II region spectrum will simply consist of recombination lines in the visible. The effect of our recalibration of the abundance scale in H II regions is shown in Figure 10.

The Alloin *et al.* (1979) [O III] $\lambda\lambda$4959, 5007/[N II] $\lambda\lambda$6548, 6584 ratio is not very useful as an abundance indicator, because it is so sensitive to the intrinsic scatter in $\bar{Q}$(H) and

TABLE 1

ADOPTED "SOLAR" ABUNDANCES

Element	Number[a]
H	12.00
He	10.93
C	8.52
N	7.68
O	8.82
Ne	7.92
Mg	7.42
Si	7.52
S	7.30
Cl	5.6
Ar	6.8

[a] Log abundance by number relative to H = 12.00.

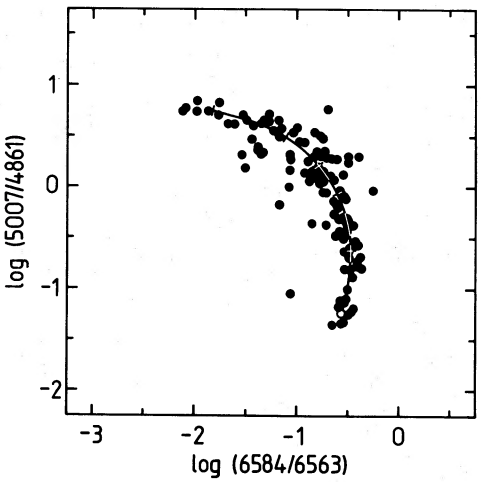

FIG. 8.—As Fig. 6, but for the third BPT figure, (5007/4861) vs. (6584/6563)

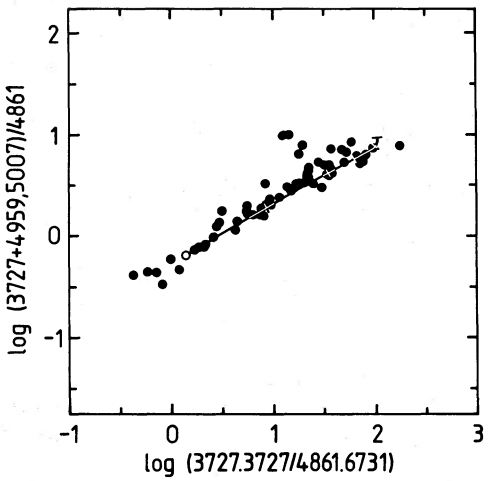

FIG. 9.—The Pagel *et al.* (1979) abundance sensitive line ratio, ([O II] λ3727 + [O III] $\lambda\lambda$4959, 5007)/Hβ, plotted against the abundance discriminant suggested in the text, (3727 · 3727/4861 · 6731), for the final theoretical sequence.

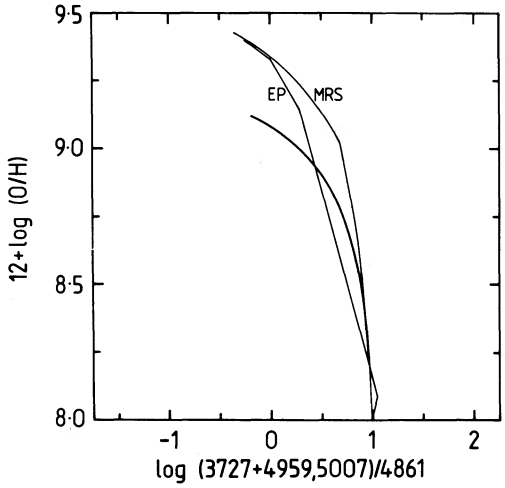

FIG. 10.—The calibration of oxygen abundance vs. the Pagel *et al.* (1979) abundance indicator ([O II] λ3727 + [O III] $\lambda\lambda$4959, 5007)/Hβ derived from the theoretical sequence. Also shown are the previous calibrations of Edmunds and Pagel (EP; 1984) and McCall, Rybski, and Shields (MRS; 1985).

because, as we discussed above, there appears to be real scatter in the N/O–O abundance relation at low abundances. This probably accounts for the large scatter in the observational points of Figure 11, in which we plot the Alloin *et al.* (1979) ratio against our abundance indicator. Nevertheless, the fit at high Z is good, which gives us confidence in the accuracy of our calibration in this regime.

As a temperature indicator, on the other hand, the Alloin *et al.* (1979) ratio is much more useful, particulary at the high abundance end. Indeed, as we indicated in the introduction, this ratio was originally intended to be used for this purpose. In Figure 12 we plot the predicted [O III] $\lambda\lambda$4959, 5007/[N II] $\lambda\lambda$6548, 6584 ratio against the mean electron temperature in the O^{++} zone, $\langle T_{[O\,III]}\rangle$, for our model sequence and for the Alloin *et al.* (1979) empirical calibration of the observational material. The fact that these are in close agreement shows that our calibration sequence predicts the correct electron temperatures, and since the temperature is critically dependent on both $\bar{Q}$(H) and Z, this agreement gives us more confidence in the $\bar{Q}$(H)–Z calibration in the high abundance limit. We regard this as important, since our recalibration of the abundance scale for H II regions differs most severely from that which is commonly adopted at the high-Z end.

VI. A METHOD FOR DERIVING CHEMICAL ABUNDANCES OF H II REGIONS

Since our sequence of models sucessfully describes the variety of H II region spectra that are observed, we are now in a position to invert the question and ask whether, from an observational measurement of only the brightest optical lines, a set of chemical abundances can be derived for a given H II region.

a) The Heavy Elements

The brightest emission lines are those of [O II], [O III], [N II], and [S II]. Thus we should aim to derive O, N, and S abundances. In Figures 13*a*–13*d*, we use our theoretical sequence to plot, as a function of oxygen abundance, the ratios ([O II] λ3727 + [O III] $\lambda\lambda$4959, 5007)/Hβ (as in Pagel *et al.*

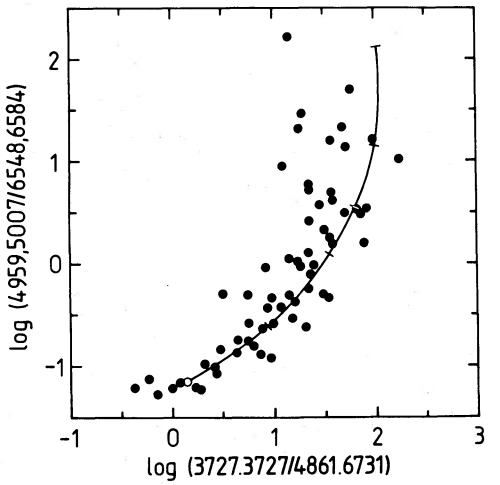

FIG. 11.—The Alloin *et al.* (ACJV; 1979) abundance sensitive line ratio [O III] $\lambda\lambda$4959, 5007/[N II] $\lambda\lambda$6548, 6584, plotted against (3727 · 3727/4861 · 6731) for the final theoretical sequence.

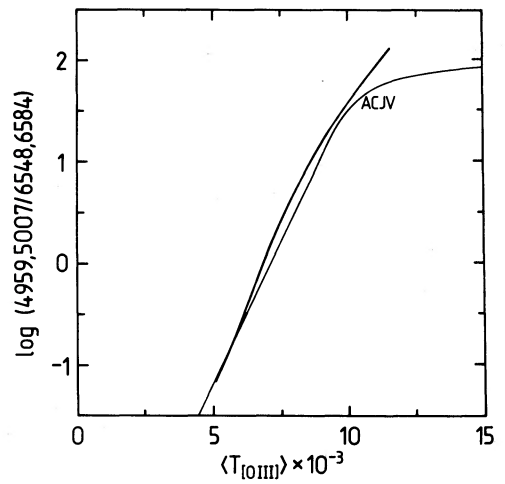

FIG. 12.—The calibration of [O III] $\lambda\lambda$4959, 5007/[N II] $\lambda\lambda$6548, 6584 vs. electron temperature in the O^{++} zone, $\langle T_{[O\,III]}\rangle$, derived from the theoretical sequence. Also shown is the calibration derived by Alloin *et al.* (1979).

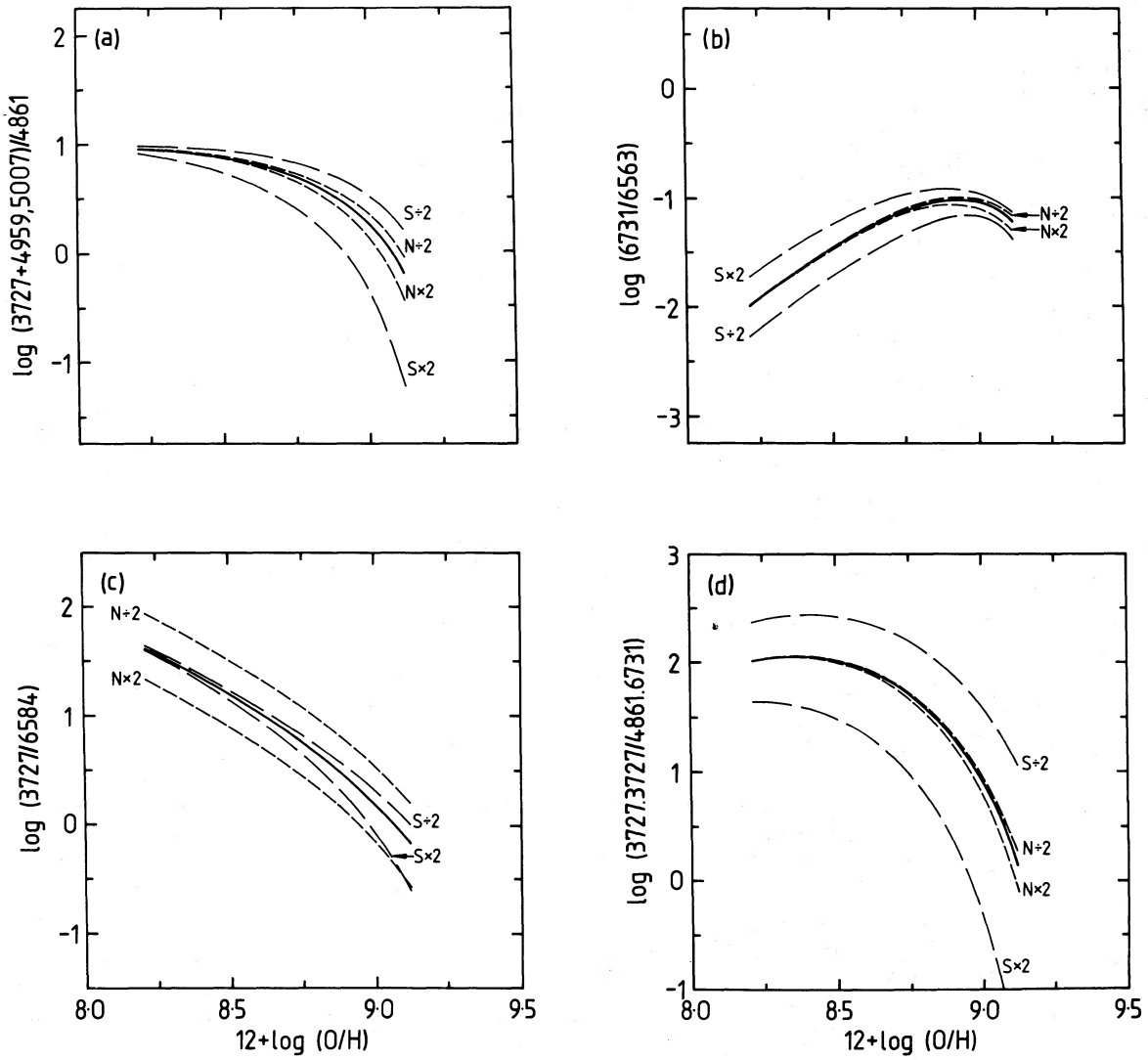

FIG. 13.—(*a*) Theoretical sequence calibration of the abundance sensitive line ratio ([O II] λ3727 + [O III] $\lambda\lambda$4959, 5007)/Hβ vs. 12 + log (O/H), (*b*) theoretical sequence calibration of the line ratio (6731/6563) vs. 12 + log (O/H), (*c*) theoretical sequence calibration of the line ratio (3727/6584) vs. 12 + log (O/H), and (*d*) theoretical sequence calibration of the line ratio (3727 · 3727/4861 · 6731) vs. 12 + log (O/H). In each figure, the adopted theoretical sequence is indicated by a solid line, while dashed lines illustrate the sequence with nitrogen or sulfur abundances increased or decreased by a factor of 2 at each point.

1979), [S II] λ6731/Hα, [O II] λ3727/[N II] λ6584, and finally our abundance indicator ratio. In each plot, the solid line depicts the theoretical sequence derived above, while the dashed lines labeled "N × 2," "N ÷ 2," "S × 2," and "S ÷ 2" indicate the sequence with nitrogen or sulfur abundances multiplied or divided by two at each point. To derive theoretical abundances from these diagrams we recommend the following procedure.

1. Use each of these ratios to derive "independent" estimates of 12 + log (O/H) from the theoretical sequence and take the mean.

2. Next, use this mean to estimate theoretical [N II] λ6584 and [S II] λ6731 line intensities from the sequence.

3. Use these theoretical values with the observed oxygen line intensities to refine the estimate of the oxygen abundance from Figures 13*a*, 13*c*, and 13*d* and iterate between steps 2 and 3 until the difference between iterations is less than 0.01 dex.

4. With this oxygen abundance, compare the predicted and observed [N II] λ6584 and [S II] λ6731 line strengths in Figures 13*c* and 13*d* to obtain the corrected nitrogen and sulfur abundances, using the scaling between the line intensity and the abundance given in the figures. Since the strength of the sulfur line is very dependent on $\bar{Q}$(H), it should be recognized that the sulfur abundance derived by this method is rather uncertain.

5. If the derived nitrogen or sulfur abundance is far from that employed in the adopted sequence, it may be necessary to iterate steps 1–4 interpolating on the figures to the correct nitrogen and sulfur abundances.

It is important to realize that the accuracy with which chemical abundances may be derived using this procedure will often be limited by the accuracy with which reddening corrections for the observational data can be determined. This is particularly true for ratios involving [O II] λ3727 for which the reddening correction is not trivial. The use of reddening corrections derived from Hβ/radio measurements is not valid because of the possible presence of regions of complete obscuration in the optical Possibly the most accurate method for deriving the [O II] λ3727 intensity is by comparison with

higher order Balmer emission lines, although this is not possible if there is appreciable underlying continuum contributing a component of Balmer absorption.

b) Helium

The helium abundance varies over a very restricted range compared to that encountered for the heavy elements. This is the justification for using a constant helium abundance in our theoretical models. If we wish to derive an accurate helium abundance, it is therefore of paramount importance to have accurate ionization correction factors (Peimbert and Torres-Peimbert 1974, 1976). These depend critically on $\bar{Q}$(H), and since $\bar{Q}$(H) and Z are correlated, then this implies that the ioinization correction factors depend on the heavy element abundance as well. In Figure 14, we plot, for our $\bar{Q}$(H)–Z correlation the theoretical variation of the line intensities relative to Hβ of the triplet 4471 and 5876 lines and the singlet 6678 line. Since there is real scatter in $\bar{Q}$(H) at a given Z, we also show the effect of varying $\bar{Q}$(H).

Another important factor which may affect the accuracy of any abundance estimate is the line transfer in the nebula. It is generally assumed that, for helium as well as hydrogen, the nebula is optically thick in the Lyman series lines (case B). This assumption is almost certainly valid for the helium triplet series, but may not be true for certain nebular geometries in the singlet lines (Brocklehurst 1971, 1972; Robbins and Robinson 1971).

The recombination coefficients are electron temperature dependent, so that in principle it is important to know this. However, in practice, this is not a problem, since the temperature dependence of the ratio of hydrogen and helium recombination lines in the optical is typically very weak (Brocklehurst 1971).

A more insidious problem is the effect of helium blanketing in the exciting star, since this directly affects the number of ionizing photons capable of ionizing helium, and therefore the extent of the zone of the nebula which contains ionized helium. However, since our sequence correctly describes the excitation of the H II regions at different metallicities, we believe that, if this effect is present, we have correctly compensated for it in our adopted $\bar{Q}$(H)–Z relationship.

On the basis of these considerations, we recommend the following procedure for the derivation of the helium abundance.

1. Having determined the heavy element abundance by the above procedure, read off the $\bar{Q}$(H) value which applies to the observed H II region using the $\bar{Q}$(H)–Z diagnostic diagrams, Figures 1, 2, or 3.

2. From Figure 14, read off the predicted line strengths of the helium lines.

3. Compute the helium abundance from each of the line ratios, assuming that the line strength scales directly as the abundance. If the value obtained for the singlet line does not agree with that obtained for the triplet lines, this is an indication that the assumption of case B may not be valid, in which case only the triplet lines should be used to derive the helium abundance and the result should be treated with caution.

Abundance estimates for individual H II regions as derived by the method proposed here are probably not very reliable, but when many H II regions are observed the method should be valid in a statistical sense. In any event, as we shall show in Paper III of this series, this method makes a useful point of departure for more detailed modeling.

VII. CONCLUSIONS

Employing the homogeneous grid of photoionization models described in Paper I, we have generated a theoretical fit to the observed spectral sequence of extragalactic H II regions. Comparison of the region of parameter space spanned by the theoretical models of Paper I with the observed distribution of H II regions demonstrates that the latter form a narrow emission-line ratio spectral sequence. In this paper, we have derived the correlation between ionization parameter and metallicity suggested in Paper I and have computed the sequence of theoretical photionization models necessary to calibrate the observed H II region spectral sequence in terms of elemental abundances.

We have established the correlation between $\bar{Q}$(H) and

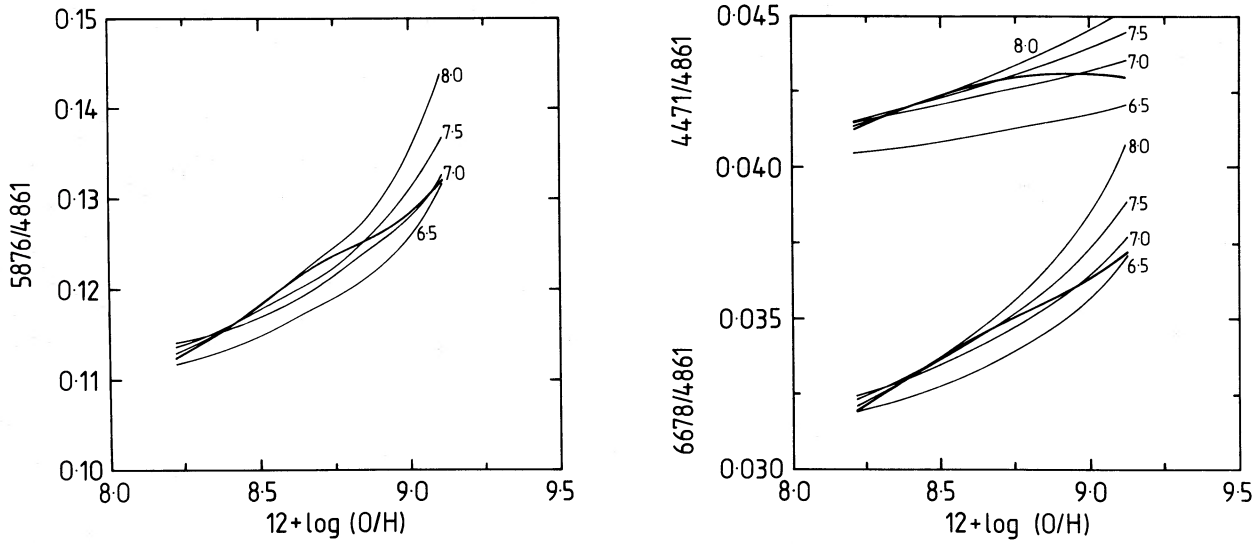

FIG. 14.—Calibration of the line ratios He I λ4471/Hβ, He I λ5876/Hβ, and He I λ6678/Hβ vs. 12 + log (O/H). Final theoretical sequence is indicated by the heavy line, while the other lines illustrate the line ratios for log $\bar{Q}$(H) = 6.5, 7.0, 7.5, and 8.0 cm s^{-1}.

oxygen abundance over the range of metallicities observed ($\sim\frac{1}{4}$–2 $Z_\odot$), and have modeled the correlation with a simple functional form which fits the observed emission line data. An explanation for the derived $\bar{Q}$(H)–Z correlation has been proposed in § IV*b*.

Comparison of the models with the observational data imply that nitrogen must be enriched as a secondary element, except at very low abundances where there is sufficient scatter in the data to suggest that there may be a primary component of nitrogen at low Z. The implications of the latter were briefly discussed in § IV*c*.

We have demonstrated that the theoretical sequence proposed in this paper reproduces the observed sequences of H II regions on a number of diagrams commonly used for excitation and abundance diagnostics, and this gives us faith in the validity of the theoretical sequence. We have employed our sequence to recalibrate the semiempirical abundance sensitive line ratios of Pagel *et al.* (1979), Edmunds and Pagel (1984), and McCall, Rybski, and Shields (1985). The major consequence of this recalibration is to change the absolute calibration of the abundance scale at high Z. For example, at a metallicity of $\sim 2\ Z_\odot$, our calibration of the oxygen abundance is $\sim$0.25 dex lower than the calibrations of Edmunds and Pagel (1984) and McCall, Rybski, and Shields (1985). Our calibration of electron temperature in the O^{++} zone agrees with that found empirically by Alloin *et al.* (1979) over much of the range of conditions observed, but our models illustrate that the Alloin *et al.* (1979) ratio is not particularly useful as an abundance discriminant because of its inherent sensitivity to the intrinsic scatter in observed $\bar{Q}$(H) and because of the scatter in the N/O–O abundance relation at low Z.

Finally, we have prescribed a method for deriving oxygen, nitrogen, and sulfur abundances from bright emission line ratios in H II regions by utilizing both previously employed abundance sensitive line ratios, together with a new abundance discriminant proposed in this paper, (3727 · 3727/4861 · 6731). We have also presented sufficient theoretical data to enable helium abundances to be derived from measurements of the intensities of He I emission lines.

In the third paper in this series, we will apply the calibration and techniques described here to derive abundances in H II regions, and the abundance gradient, in the bright northern spiral galaxy M101.

We wish to thank the Anglo-Australian Observatory for use of their computing facilities in calculating many of the models described here. We also wish to thank the referee, John Mathis, for many valuable suggestions for improving the quality of this paper. One of us (I. N. E.) acknowledges the receipt of an Australian Commonwealth Postgraduate Research Award.

REFERENCES

Alloin, D., Collin-Souffrin, S., Joly, M., and Vigroux, L. 1979, *Astr. Ap.*, **78**, 200.
Baldwin, J. A., Phillips, M. M., and Terlevich, R. 1981, *Pub. A.S.P.*, **93**, 5 (BPT).
Brocklehurst, M. 1971, *M.N.R.A.S.*, **153**, 471.
———. 1972, *M.N.R.A.S.*, **157**, 211.
Clegg, R. E. S., Lambert, D., and Tomkin, J. 1981, *Ap. J.*, **250**, 262.
Dennefeld, M., and Stasińska, G. 1983, *Astr. Ap.*, **118**, 234.
Dopita, M. A., Binette, L., D'Odorico, S., and Benvenuti, P. 1984, *Ap. J.*, **276**, 653.
Dufour, R. J. 1975, *Ap. J.*, **195**, 315.
———. 1977, *Ap. J.*, **216**, 706.
Dufour, R. J., Shields, G. A., and Talbot, R. J. 1982, *Ap. J.*, **252**, 461.
Dufour, R. J., Talbot, R. J., Jensen, E. B., and Shields, G. A. 1980, *Ap. J.*, **236**, 119.
Edmunds, M. G., and Pagel, B. E. J. 1978, *M.N.R.A.S.*, **185**, 77P.
———. 1984, *M.N.R.A.S.*, **211**, 507.
Evans, I. N. 1986, *Ap. J.*, **309** (Paper III).
Evans, I. N., and Dopita, M. A. 1985, *Ap. J. Suppl.*, **58**, 125 (Paper I).
Hummer, D. G., and Mihalas, D. M. 1970, *M.N.R.A.S.*, **147**, 339.
Kaler, J. B. 1981, *Ap. J.*, **244**, 54.
Lequeux, J., Peimbert, M., Rayo, J. F., Serrano, A., and Torres-Peimbert, S. 1979, *Astr. Ap.*, **80**, 155.
Martin, P. G., and Ferland, G. J. 1980, *Ap. J.* (*Letters*), **235**, L125.
Mathis, J. S., Chu, Y.-H., and Peterson, D. E. 1985, *Ap. J.*, **292**, 155.
McCall, M. L. 1982, Ph.D. thesis, University of Texas.
McCall, M. L., Rybski, P. M., and Shields, G. A. 1985, *Ap. J. Suppl.*, **57**, 1.
Nomoto, K., Thielemann, F.-K., and Yokoi, K. 1984, *Ap. J.*, **286**, 644.
Pagel, B. E. J., and Edmunds, M. G. 1981, *Ann. Rev. Astr. Ap.*, **19**, 77.
Pagel, B. E. J., Edmunds, M. G., Blackwell, D. E., Chun, M. S., and Smith, G. 1979, *M.N.R.A.S.*, **189**, 95.
Pagel, B. E. J., Edmunds, M. G., Fosbury, R. A. E., and Webster, B. L. 1978, *M.N.R.A.S.*, **184**, 569.
Pagel, B. E. J., Edmunds, M. G., and Smith, G. 1980, *M.N.R.A.S.*, **193**, 219.
Peimbert, M., and Costero, R. 1969, *Bol. Obs. Tonantzintla y Tacubaya*, **5**, 3.
Peimbert, M., and Torres-Peimbert, S. 1974, *Ap. J.*, **193**, 327.
———. 1976, *Ap. J.*, **203**, 581.
Petrosian, V., Silk, J., and Field, G. B. 1972, *Ap. J.* (*Letters*), **177**, L69.
Renzini, A., and Voli, M. 1981, *Astr. Ap.*, **94**, 175.
Robbins, R. R., and Robinson, E. L. 1971, *Ap. J.*, **167**, 249.
Sarazin, C. L. 1976, *Ap. J.*, **208**, 323.
———. 1977, *Ap. J.*, **211**, 772.
Searle, L. 1971, *Ap. J.*, **168**, 327.
Shields, G. A., and Searle, L. 1978, *Ap. J.*, **222**, 821.
Smith, H. E. 1975, *Ap. J.*, **199**, 591.
Stasińska, G. 1980, *Astr. Ap.*, **84**, 320.
Talbot, R. J., and Arnett, W. D. 1974, *Ap. J.*, **190**, 605.
Weaver, T. A., Zimmerman, G. B., and Woosley, S. E. 1978, *Ap. J.*, **225**, 1021.
Woosley, S. E., and Weaver, T. A. 1982, in *Essays in Nuclear Astrophysics*, ed. C. A. Barnes (Cambridge: Cambridge University Press), p. 377.

MICHAEL A. DOPITA and IAN N. EVANS: Mount Stromlo and Siding Spring Observatories, Private Bag, Woden P.O., ACT 2606, Australia